Tuning the DARHT Long-Pulse Linear Induction Accelerator

Carl Ekdahl, *Senior Member, IEEE*

***Abstract*— Flash radiography of large hydrodynamic experiments driven by high explosives is a well-known diagnostic technique in use at many laboratories. The Dual-Axis Radiography for Hydrodynamic Testing (DARHT) facility at Los Alamos produces flash radiographs of large hydrodynamic experiments. Two linear induction accelerators (LIAs) make the bremsstrahlung radiographic source spots for orthogonal views of each test. The 2-kA, 20-MeV Axis-I LIA creates a single 60-ns radiography pulse. The 1.7-kA, 16.5-MeV Axis-II LIA creates up to four radiography pulses by kicking them out of a longer pulse that has a 1.6-μs flat top. The DARHT LIAs use solenoidal focusing for transport of the beam through the accelerators. The long-pulse Axis-II LIA has 74 accelerating cells, and uses 91 solenoids and 80 pairs of dipoles for focusing, transporting, and steering the beam. The setting of the currents of these 251 magnets is called tuning the accelerator. Tuning is done in two stages. First, the solenoidal focusing magnets are set to values designed to provide a beam with minimal envelope oscillations, and little or no instability growth. Then, steering dipoles are adjusted to minimize the low-frequency motion of the beam centroid and center it at the LIA exit. The design of the focusing tune is computationally intensive. Focusing tune design methods, simulations, and validation are the main topics of this article.**

***Index Terms*— Beam dynamics, beam focusing, beam transport, linear induction accelerators (LIAs).**

I. Introduction

FLASH radiography of large hydrodynamic experiments driven by high explosives is a well-known diagnostic technique in use at many laboratories. At Los Alamos, the Dual-Axis Radiography for Hydrodynamic Testing (DARHT) facility produces multiple flash radiographs from different directions of hydrodynamic experiments. Two linear induction accelerators (LIAs) make the bremsstrahlung radiographic source spots for orthogonal views of each test. The 2-kA, 20-MeV Axis-I LIA creates a single 60-ns radiography pulse. The 1.7-kA, 16.5-MeV Axis-II creates multiple radiography pulses by kicking them out of a longer pulse from the LIA that has a 1.6-μs flattop (Fig. 1). The Axis-II injector, LIA, kicker, and downstream transport (DST) to the bremsstrahlung converter are described in [1]–[5].

The DARHT Axis-II injector and LIA use solenoids for focusing the beam and dipole pairs for steering. Each cell incorporates a solenoid and a colocated pair of dipoles. Including all magnets in between blocks of cells, in the diode anode region, and elsewhere, there are 91 solenoids and 80 pairs of dipoles. These magnets must be adjusted to produce a well-centered and matched beam, with negligible motion from instabilities or other effects, and minimal emittance growth in the LIA. Adjusting the magnetic focusing and steering magnets to optimize the electron-beam transport through an LIA is often called "tuning." Thus, a total of 251 individual magnets must be set to tune the Axis-II injector and LIA.

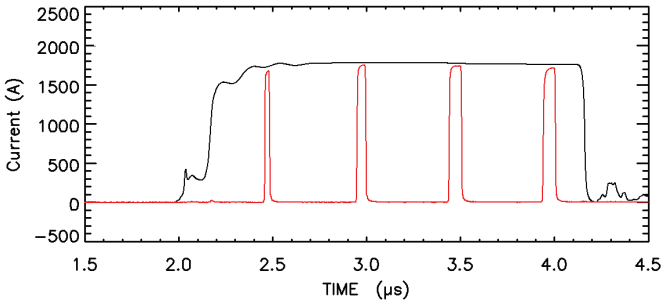

Fig. 1. DARHT Axis-II beam current. Black line: long current pulse measured at LIA exit. Red line: four short-kicked pulses delivered to the radiography Bremsstrahlung conversion target.

Tuning the Axis-II injector and LIA is done in two stages. First, the solenoidal focusing magnets are set to values designed to provide a beam with minimal envelope oscillations, and little or no beam-breakup (BBU) instability growth. Then, steering elements are adjusted to minimize the low-frequency motion of the beam centroid and center it at the LIA exit.

In solenoidal transport, a smoothly varying beam size can be found for which radial forces balance, and the beam is said to be "matched" to the focusing field. A "mismatched" beam exhibits unwanted oscillations in size, which are a source of free energy that contributes to emittance growth. Such oscillations are highly undesirable, because in the absence of beam-target effects, the radiographic spot size is proportional to the emittance.Therefore, our focusing tunes pay particular attention to matching the beam to minimize envelope oscillations, while simultaneously minimizing motion of the beam centroid. A typical tune is shown in Fig. 2, which illustrates the use of the first block of cells downstream of the apertures to match the beam to the high magnetic fields in the main LIA, and subsequent transport of the well-matched beam.

As seen in Fig. 2, the beam tube is substantially larger than the beam during the pulse flat top. The large tube sizes

Manuscript received January 2, 2013; revised February 25, 2013; accepted March 30, 2013. Date of publication July 3, 2013; date of current version October 7, 2013. This work was supported by the U.S. Department of Energy under Contract DE-AC52-06NA25396.

The author is with Los Alamos National Laboratory, Los Alamos, NM 87545 USA (e-mail: cekdahl@lanl.gov).

Color versions of one or more of the figures in this paper are available online at http://ieeexplore.ieee.org.

Digital Object Identifier 10.1109/TPS.2013.2256933

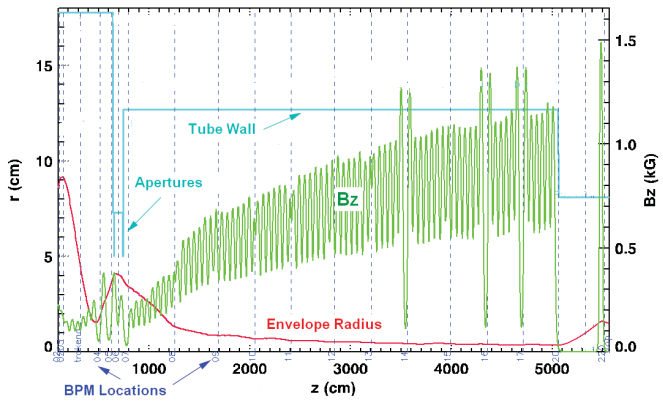

Fig. 2. Envelope code simulation of beam transport through the injector cell block and into the main LIA. Green line: the solenoidal focusing magnetic field strength on axis (legend on right). Red line: the beam envelope radius, r, during the flat-top of the long beam pulse shown in Fig. 1. Light Blue line: the beam tube radius. Blue dashed line: locations of beam position monitors.

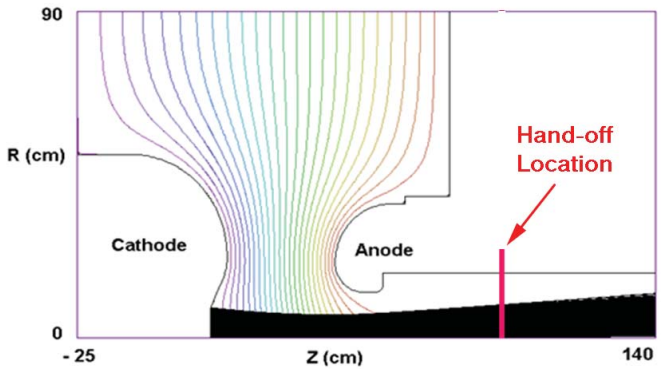

Fig. 3. TRAK gun-design code simulation of 1.7-kA space-charge limited current produced by the hot dispenser cathode in the Axis-II diode when biased to 2.2 MV. The initial conditions for the envelope codes obtained at the position of the vertical red line (z = 100 cm) were $r_0 = 8.8$ cm and $r_0' = 24.7$ mr. The normalized emittance at that location calculated from TRAK simulations was 178 π-mm-mr.

were chosen to reduce risk from beam spill onto accelerating gaps, and mitigation of the resistive wall instability, which is dangerous for long-pulse accelerators. During the long risetime (at low energy), the beam envelope has large oscillations. Beam spill into the accelerating gaps during the risetime is prevented by the use of the large beam tubes. Moreover, the use of large tubes mitigates the resistive wall instability, which has a growth rate inversely proportional to the cube of the tube size [4].

High-frequency centroid motion (ns time-scales) would enlarge the effective radiographic source spot through time integrated blurring. A major source of high-frequency motion in LIAs is the BBU instability. Our tunes suppress BBU by using large solenoidal fields [3]. The tune shown in Fig. 2 suppressed the BBU to less than 1% of the beam diameter.

Slow centroid motion (μs time scales) would produce spot to spot displacements. Slow motion in DARHT Axis-II is caused by the pulsed-power variation interacting with dipoles resulting from asymmetric injection and cell misalignment [4]. Since this slow motion is exacerbated by high solenoidal fields, our tunes use only the minimum field strength to suppress BBU to acceptable levels, and no more. Using a few of the steering dipoles with the tune shown in Fig. 2, we were able to reduce the slow motion to less than 10% of the beam diameter [4].

Section II covers the general approach to design of focusing solenoid tunes for the DARHT Axis-II injector and LIA. Section III presents some evidence for the validity of the simulations used for design of the focusing tune. In Section IV, we discuss simulations intended to provide insight into the vulnerability of our tunes to the growth of emittance in the LIA. We provide a brief discussion of the methods we use to suppress centroid motion in Section V; details are readily available in [3] and [4].

II. Tune Design Simulations

Designing a focusing tune for DARHT relies heavily on a number of beam dynamics simulation codes. The primary tools are the XTR and LAMDA codes, which solve the second-order differential equations for the beam envelope [6]–[13]. Since these envelope codes are second-order differential equation solvers, they require the envelope radius and divergence at the exit of the diode as initial conditions.

Unlike many other LIAs, we have no direct measurements of the properties of the beam as it exits the diode, because this region is inaccessible due to the massive (6-ton) injector cells. Therefore, we must rely on computer simulations of the diode to provide these initial conditions. Space-charge limited diode simulations were performed in 2-D using the TRICOMP suite of codes [14]–[16], which include TRAK. The results of the TRAK simulations were substantially in agreement with simulations of the same geometry and applied magnetic fields using the LSP particle-in-cell (PIC) code. Beam parameters obtained from these simulations are used to initialize XTR and LAMDA. The initial conditions, the space-charge limited current, and the normalized emittance were obtained from simulations with anode–cathode (A–K) voltages ranging from 100 kV to 2.8 MV, so that XTR and LAMDA could be used to predict beam behavior during the long, ~500–ns beam rise time [1], [2].

Fig. 3 illustrates a TRAK simulation of the DARHT Axis-II diode, showing the equipotentials and the space-charge limited electron beam at maximum current. The initial conditions for XTR and LAMDA determined from TRAK at ~80-cm downstream from the cathode surface, (Z = 100 cm) were $r_0 = 8.8$ cm and $r_0' = 24.7$ mr. The normalized emittance at that location was 178 π-mm-mr from the TRAK simulation.Using these initial conditions, a tune was designed with XTR resulting in the predicted beam envelope shown in Fig. 2.

A code that we use extensively for tuning both DARHT LIAs is the XTR envelope code written by Paul Allison [9], [10]. XTR solves for the beam envelope radius and its first spatial derivative, the envelope divergence, as functions of position. The initial parameters required by XTR at the beginning of the integration are the beam kinetic energy, the beam current, the beam emittance, and the two initial conditions: radius and divergence. The initial beam kinetic

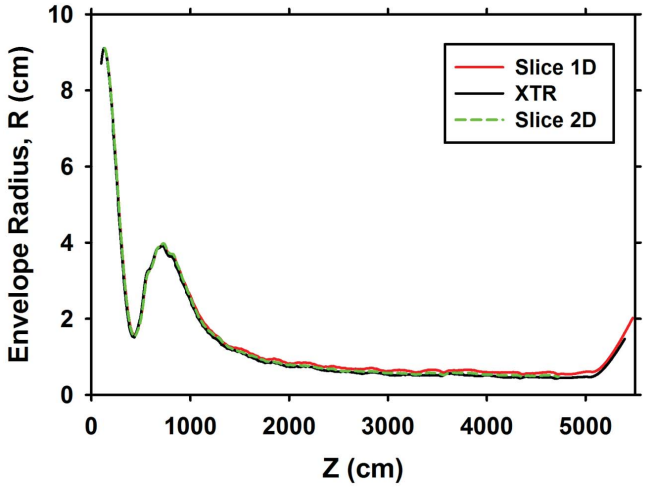

Fig. 4. Comparison of two LSP-based PIC slice codes [19] with the XTR envelope code. All three simulations used the same magnetic focusing fields and initial conditions.

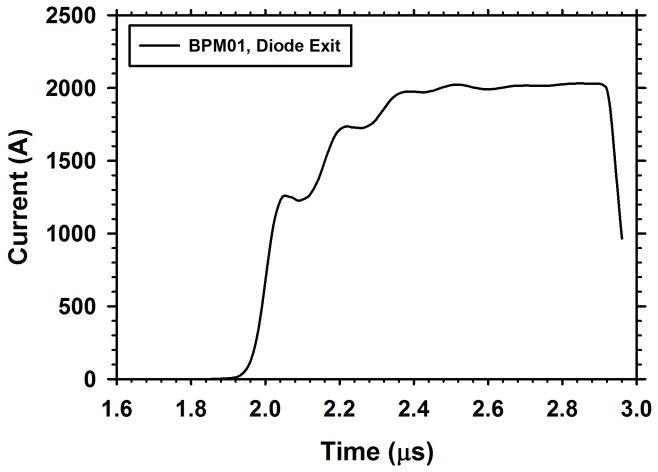

Fig. 5. Measured beam current through the diode anode showing the ~500-ns risetime with 6.5-MHz LC oscillations resulting from the high-voltage feed geometry [2]. The pulse is sharply terminated by the crowbar switch.

energy is that acquired by acceleration through the diode AK gap. Also required is a model of the accelerator that includes locations and values for accelerating gaps, locations and energizing currents for focusing solenoids, and beam tube and aperture sizes. Acceleration is calculated from a thin lens model of the potential in the gaps. The solenoidal focusing field in XTR is calculated from solenoid models that have parameters fit to experimental measurements.

We also use the LAMDA envelope code, which has the additional capability of modeling the time-resolved transport of a realistic beam-pulse waveform [11], [12]. LAMDA does this by subdividing the beam pulse into slices, which are each treated as time-independent, and disconnected, envelopes; a technique that has been shown to agree with very complex experiments [13]. Both XTR and LAMDA have higher order corrections to the simple envelope equations derived in [6]–[8] to account for space-charge potential depression in the beam and the beam diamagnetism. LAMDA and XTR have been extensively compared with each other, and they agree in all cases examined [17].

III. Validation of Simulations

Since the focusing tune is so heavily dependent on simulations we have challenged these in every way practical in order to gain confidence in their results. For example, we have compared the results of the envelope codes with each other [17], with TRAK, and with PIC codes [17], [18]. Fig. 4 shows a comparison of the envelope calculated with XTR and compared with the results of PIC code simulations with slice codes based on LSP. Two slice models have been used; Slice "1-D" models a centered beam in cylindrical coordinates, and Slice "2-D" uses Cartesian coordinates to be able to simulate the motion of the beam centroid, and to fully resolve the transverse-phase space [19].

Although these code comparisons are encouraging, especially considering the physical approximations inherent in the envelope codes, we compare code predictions with experimental data wherever practical. For example, time-resolved beam images obtained after the accelerator exit have agreed with code predictions to well within experimental error for several different configurations of the Axis-II accelerator [2], [20], [21].

We have also compared the diode simulations with experimental data. The long beam risetime provides an opportunity to make comparisons of experimental data with simulations over a broad range of energies. Fig. 5 shows the measured beam current exiting the diode for a recent shot, illustrating the long off-energy risetime and LC oscillations caused by the large inductances and capacitances in the high-voltage feed for the diode. The pulse is terminated by a diverter switch called the "crowbar" (C/B). At the diode exit, the risetime contains all energies up to the diode anode–cathode potential (V_{AK}). After exiting the diode, the beam is accelerated through six injector cells, having large beam tube radius of 19 cm, and with solenoids set to prevent beam envelope oscillations from exceeding ¾ of the tube size at any energy in the beam risetime. The beam then transitions through a section with apertures that remove some of the beam risetime current, and then it is matched to the field of the main LIA, which has a smaller tube radius of 12.7 cm. These features are shown in Fig. 2.

One experimental test of the TRAK simulations is to compare the measured diode current and voltage with the simulation results. This comparison is shown in Fig. 6, which includes all of the data for the pulse shown in Fig. 5 for which the diode AK voltage was greater than 100 kV; thus energies ranging from nonrelativistic to full-relativistic. It includes experimental data from both the slow risetime beam head and the fast C/B-initiated falltime. The agreement between simulation and experiment is within measurement uncertainty over the full range of beam energies.

The envelope simulations of the beam accelerated through the injector cells have also been experimentally validated over a wide range of beam parameters. As described earlier, *in lieu* of experimental measurements, we rely on TRAK gun-design simulations of the diode to provide the initial conditions for the XTR or LAMDA envelope codes.

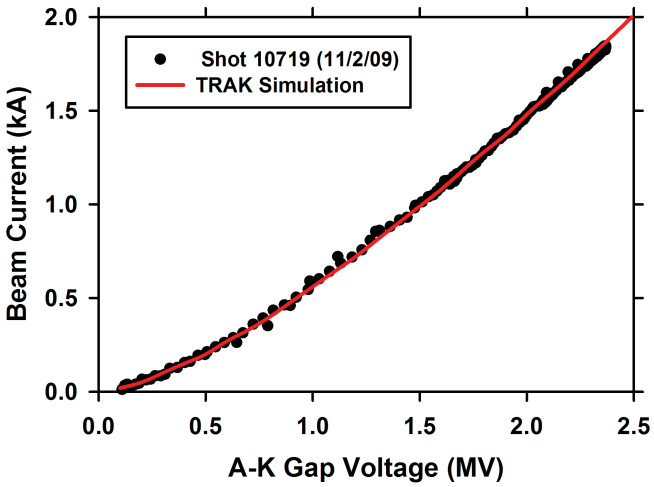

Fig. 6. Diode current–voltage characteristic curve as measured experimentally compared with the curve generated from TRAK simulations. The experimental data cover the entire pulse shown in Fig. 5 for which the AK voltage was greater than 100 kV. Thus, the plot compares data and simulation from nonrelativistic to relativistic energies.

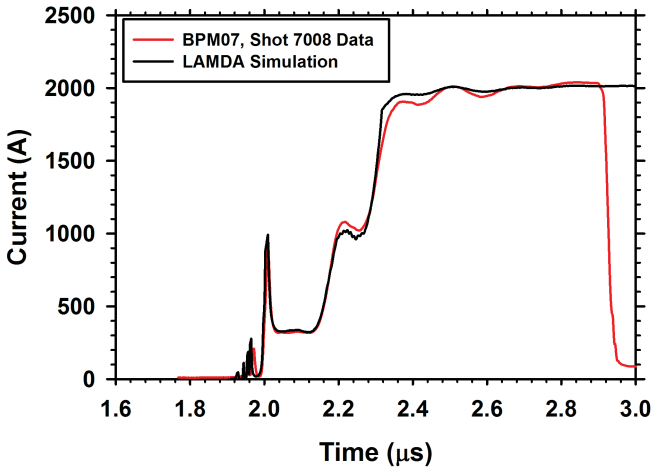

Fig. 7. Current transmitted through the apertures shown in Fig. 2. Compare with diode current in Fig. 5 to see how off-energy beam in risetime is scraped off by the apertures. Red line: the shorter pulse is data from shot 7008 from the first BPM beyond the apertures. Black line: the longer pulse is the result of a LAMDA simulation. The LAMDA simulation used time varying initial conditions derived from TRAK simulations of the diode at AK voltages ranging from 100 kV to 2.8 MV.

Another way to experimentally confirm this procedure is to measure the current passed through the apertures shown in Fig. 2 during the off-energy beam risetime. During this time, the beam has a continuously varying envelope, some of which is scraped off by the apertures. This causes a time-dependent variation of the transmitted current, and to the extent that the envelope calculation using TRAK-derived initial conditions agrees with the experimental data, we can validate this approach. Fig. 7 shows such a comparison between the LAMDA envelope simulation of apertured current and the current measured just downstream of the apertures. The agreement between the theory and experiment seen in the figure lends confidence in using TRAK to establish initial conditions for the envelope codes. The agreement also demonstrates the envelope codes' ability to accurately predict the size of an obviously nonparaxial beam between the diode exit and the apertures (see Fig. 2).

Finally, whenever we have had an opportunity to image the beam at the exit of any of the many versions of the DARHT Axis-II accelerator, the size of the beam has agreed with XTR envelope code simulations to within experimental uncertainty [2], [20], [21].

IV. Emittance Growth

We used the PIC slice codes based on LSP to investigate the vulnerability of our tunes to emittance growth. One of the requirements of our tunes is that they produce a matched beam with little or no envelope oscillations during the flat top. A badly mismatched beam exhibits large envelope oscillations, sometimes called a "sausage," "m = 0," or "breathing" mode. The free energy in these oscillations feeds the growth of emittance [22]. The detailed mechanism of this contribution to emittance growth is parametric amplification of electron orbits that resonate with the envelope oscillation, expelling those electrons from the beam core into a halo [23], [24].

Another well-known contributor to emittance growth in solenoidal focusing systems is cumulative spherical aberration

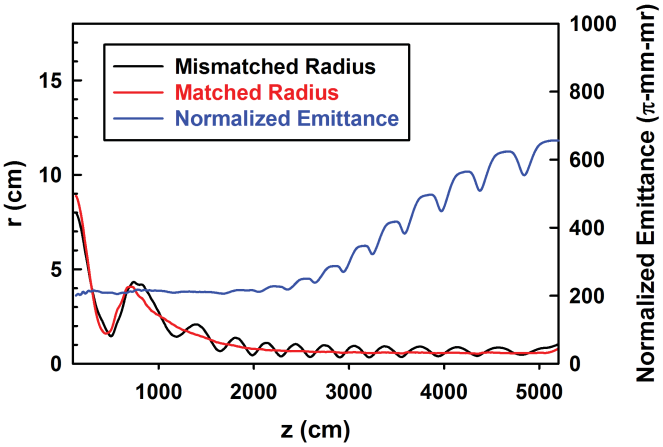

Fig. 8. Red line: envelope radius of a matched beam. Black line: envelope radius of a mismatched beam. Blue line: the emittance of the mismatched beam simulated by the Slice 1-D PIC code shows substantial growth through the LIA.

[22], [25], which also over-focuses the edge of the beam, producing hollow beam profiles [26]. However, even though the cumulative spherical aberration is large in our LIA, and the resulting edge focusing is evident in PIC simulations, the resulting emittance growth is small because the beam is rapidly focused to a size much smaller than the bore of the solenoids. Essentially all of the emittance growth observed in our PIC code simulations appears to come from the parametric amplification of orbits by envelope oscillations, so the design of our tunes emphasizes transport of a well-matched beam.

Emittance growth was calculated using LSP PIC code simulations that model a slice of the beam as it transports through the accelerator. There was no growth in the main accelerator for a matched beam, even though there is appreciable cumulative spherical aberration in the LIA. The only growth from the initial diode emittance was ~10% increase in the injector cells, where the beam is large (Fig. 2). These simulations produced considerable emittance growth when the

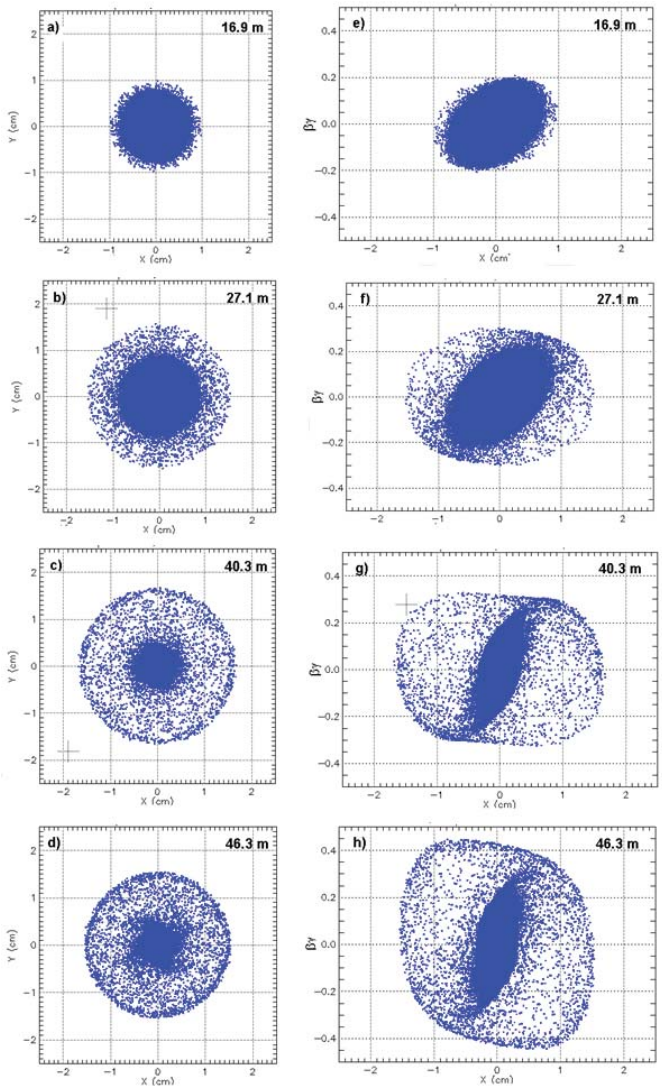

Fig. 9. (a)–(d) Configuration space (x,y) showing growth of halo as mismatched beam propagates through LIA (top to bottom). (e)–(h) Phase space (x,px) showing resonant particle ejection into the halo, with a correspondingly larger momentum ($\beta\gamma$) contribution to emittance as the beam propagates through the LIA.

beam was highly mismatched (Fig. 8). This was accompanied by damping of the envelope oscillations as the oscillation energy was randomized. That the emittance growth is due to parametric amplification of resonant orbits producing a halo is confirmed through examination of the evolution of configuration and phase space snapshots of the beam slice as it transports through the LIA (Fig. 9). Finally, no emittance growth resulted from a matched beam that was initially offset by as much as 1 cm. The ensuing helical motion through the solenoidal guide field did not appear to contribute to emittance growth, at least in these PIC code simulations.

Fortunately, our tunes are somewhat resilient to this emittance growth mechanism. The first few solenoids in the main LIA (Fig. 2) can be used to significantly reduce the oscillations and emittance growth from an initial mismatch. Moreover, mismatched beams with relative oscillation amplitudes ($A \equiv \Delta R/\bar{R}$) as large as 50% caused less than $\sim$8% emittance growth, as shown in Fig. 10. However, as evidenced by Fig. 10,

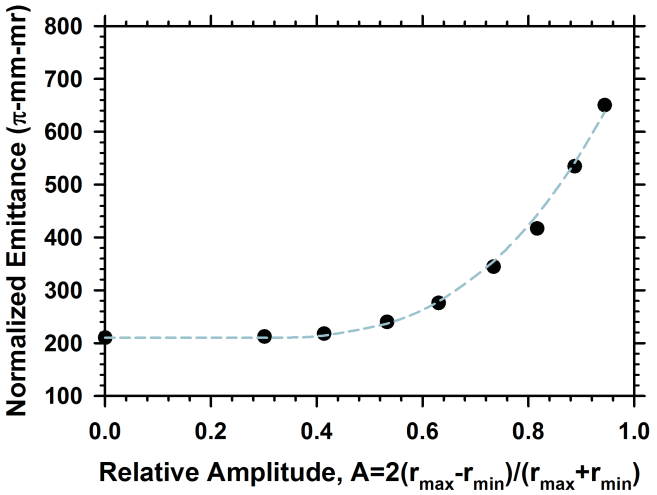

Fig. 10. Emittance at the exit of the LIA (z $\sim$ 52 m) as a function of the relative envelope oscillation amplitude near the beginning of observable growth (z $\sim$ 31 m). The light blue dashed line is simply an interpolating function.

these simulations clearly show that larger envelope oscillation amplitudes cause noteworthy emittance growth.

V. Tuning Out Beam Motion

Beam motion in the accelerator would be anathema for multipulse flash radiography. High-frequency motion, such as from BBU instability, would blur the individual spots. Low-frequency motion, such as that produced by pulsed power variation, would produce spot to spot differences.

High-frequency beam motion, with period less than the kicked pulsewidth, would increase the radiographic source spot size by integrating the position over the pulsewidth. The major source of high-frequency motion in our LIA is the BBU instability. BBU results from beam coupling of accelerating-cell TM_{1n0} modes. Since the Axis-II cells have TM mode resonances higher than 100 MHz, large-amplitude BBU instability would blur the spots of our many-ns radiographic pulses. Therefore, we have taken precautions to suppress this instability both through the design and construction of the cells and through the tuning of the accelerator focusing fields. Reference [3] details our extensive experiments to validate BBU theory on this LIA, and [4] describes recent results; the BBU peak-to-peak amplitude at the LIA exit is suppressed by the high solenoidal focusing field to less than 0.1 mm, as shown in Fig. 11.

Low-frequency beam motion, with a period greater than the kicked pulse FWHM, would result in displacement of the centers of successive radiographic source spots. Each pulse has enough energy density to erode the converter target, so displacement of early pulses in a sequence could lead to azimuthally asymmetric target material and distorted spots for the later pulses. Uncorrected beam motion at the exit of the Axis-II LIA was substantial, and would have caused the radiographic source spots to meander by more than their size. The sources of this motion are asymmetric injection from the diode into the solenoidal focusing field, solenoid misalignment in the LIA, and small temporal variation in accelerating potentials. We use the steering dipoles to suppress

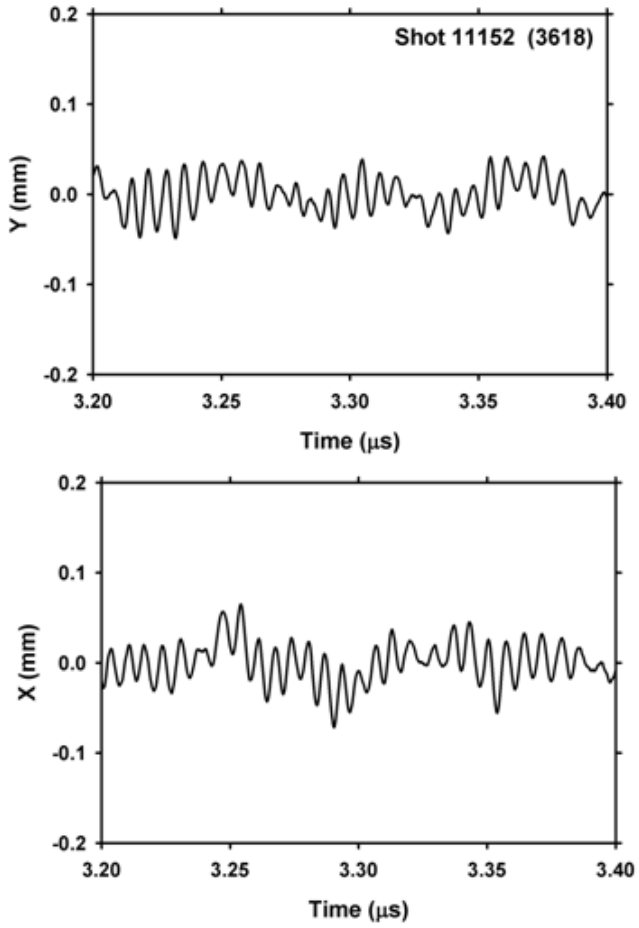

Fig. 11. BBU amplitude at the exit of the LIA is less than ∼0.1 mm peak-to-peak, which is less than ∼2% of the beam envelope radius predicted by XTR.

this motion at the LIA exit to less than 1 mm over the four-pulse radiographic format; the methods we use to do this are detailed in [4].

Fig. 12 shows the position of the beam centroid at the LIA exit at the times of the four radiographs of a recent experiment. The dashed circle in the figure depicts the beam envelope predicted by XTR for reference.

ACKNOWLEDGMENT

The author would like to thank the expert DARHT technical staff and operations crew for implementing the tunes designed with these simulations, and providing the data for validation. He would also like to thank the intellectual stimulation of a multitude of interesting discussions with numerous colleagues during the commissioning and tuning of the DARHT Axis-II LIA since first beam in 2002. Especially appreciated are technical conversations with J. Johnson, B. T. McCuistian, D. Moir, K. Nielsen, C. Rose, and M. Schulze.

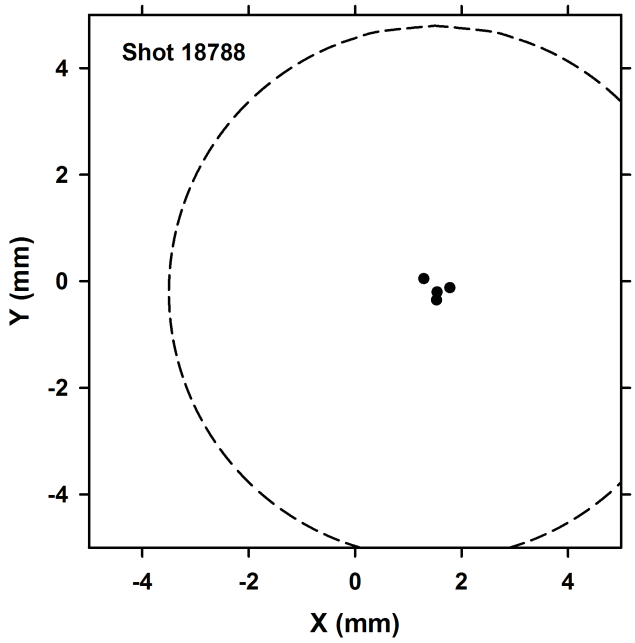

Fig. 12. Black dots: positions of the beam centroid at the LIA exit at the times of the four radiographs of a recent hydrodynamic experiment. Dashed circle: XTR prediction of the beam envelope at this position.

REFERENCES

[1] C. Ekdahl, E. O. Abeyta, L. Caudill, K. C. D. Chan, D. Dalmas, S. Eversole, R. Gallegos, J. Harrison, M. Holzscheiter, J. Johnson, E. Jacquez, B. T. McCuistian, N. Montoya, K. Nielsen, D. Oro, L. Rodriguez, P. Rodriguez, M. Sanchez, M. Schauer, D. Simmons, H. V. Smith, J. Studebaker, G. Sullivan, C. Swinney, R. Temple, Y. J. Chen, T. Houck, E. Henestroza, S. Eylon, W. Fawley, S. S. Yu, H. Bender, W. Broste, C. Carlson, G. Durtschi, D. Frayer, D. Johnson, K. Jones, A. Meidinger, K. Moy, R. Sturgess, C. Y. Tom, T. Hughes, and C. Mostrom, "First beam at DARHT-II," in *Proc. Part. Accel. Conf.*, vol. 1. Portland, OR, USA, May 2003, pp. 558–562.

[2] C. Ekdahl, E. O. Abeyta, H. Bender, W. Broste, C. Carlson, L. Caudill, K. C. D. Chan, Y. J. Chen, D. Dalmas, G. Durtschi, S. Eversole, S. Eylon, W. Fawley, D. Frayer, R. Gallegos, J. Harrison, E. Henestroza, M. Holzscheiter, T. Houck, T. Hughes, S. Humphries, D. Johnson, J. Johnson, K. Jones, E. Jacquez, B. T. McCuistian, A. Meidinger, N. Montoya, C. Mostrom, K. Moy, K. Nielsen, D. Oro, L. Rodriguez, P. Rodriguez, M. Sanchez, M. Schauer, D. Simmons, H. V. Smith, J. Studebaker, R. Sturgess, G. Sullivan, C. Swinney, R. Temple, C. Y. Tom, and S. S. Yu, "Initial electron-beam results from the DARHT-II linear induction accelerator," *IEEE Trans. Plasma Sci.*, vol. 33, no. 2, pp. 892–900, Apr. 2005.

[3] C. Ekdahl, E. O. Abeyta, P. Aragon, R. Archuleta, R. Bartsch, H. Bender, R. Briggs, W. Broste, C. Carlson, K. C. D. Chan, D. Dalmas, S. Eversole, D. Frayer, R. Gallegos, J. Harrison, T. Hughes, E. Jacquez, D. Johnson, J. Johnson, B. T. McCuistian, N. Montoya, C. Mostrom, S. Nath, D. Oro, L. Rowton, M. Sanchez, R. Scarpetti, M. Schauer, M. Schulze, Y. Tang, A. Tipton, and C. Y. Tom, "Long-pulse beam stability experiments on the DARHT-II linear induction accelerator," *IEEE Trans. Plasma Sci.*, vol. 34, no. 2, pp. 460–466, Apr. 2006.

[4] C. Ekdahl, E. O. Abeyta, P. Aragon, R. Archuleta, R. Bartsch, H. Bender, R. Briggs, W. Broste, C. Carlson, K. C. D. Chan, D. Dalmas, S. Eversole, D. Frayer, R. Gallegos, J. Harrison, T. Hughes, E. Jacquez, D. Johnson, J. Johnson, B. T. McCuistian, N. Montoya, C. Mostrom, S. Nath, D. Oro, L. Rowton, M. Sanchez, R. Scarpetti, M. Schauer, M. Schulze, Y. Tang, A. Tipton, and C. Y. Tom, "Suppressing beam-centroid motion in a long-pulse linear induction accelerator," *Phys. Rev. Special Topics Accel. Beams*, vol. 14, no. 12, pp. 120401-1–120401-8, Dec. 2011.

[5] M. Schulze, E. O. Abeyta, R. Archuleta, J. Barazza, D. Dalmas, C. Ekdahl, W. Gregory, J. Harrison, J. Johnson, E. Jacquez, P. Marroquin, B. T. McCuistian, R. Mitchell, N. Montoya, S. Nath, K. Nielson, R. Ortiz, L. Rowton, R. Scarpetti, G. Seitz, M. Schauer, R. Anaya, G. Caporaso, F. Chambers, Y. J. Chen, S. Falabella, G. Guethlein, B. Raymond, R. Richardson, J. Watson, J. Weir, H. Bender, W. Broste, C. Carlson, D. Frayer, D. Johnson, C. Y. Tom, T. P. Hughes, and C. Thoma, "Commissioning the DARHT-II accelerator downstream transport and target," in *Proc. Linear Accel. Conf.*, Victoria, BC, USA, Sep. 2008, pp. 427–429.

[6] E. P. Lee and R. K. Cooper, "General envelope equation for cylindrically symmetric charged-particle beams," *Part. Accel.*, vol. 7, no. 2, pp. 83–95, 1976.

[7] M. Reiser, *Theory and Design of Charged Particle Beams*. New York, NY, USA: Wiley, 1994, p. 202.
[8] S. Humphries, *Charged Particle Beams*. New York, NY, USA: Wiley, 1990, p. 400.
[9] P. Allison, "Beam dynamics equations for XTR," Los Alamos Nat. Lab., Alamos, NM, USA, Rep. LA-UR-01-6585, 2001.
[10] T. P. Hughes, D. C. Moir, and P. W. Allison, "Beam injector and transport calculations for ITS," in *Proc. Particle Accel. Conf.*, Dallas, TX, USA, 1995, pp. 1207–1209.
[11] T. C. Genoni, T. P. Hughes, and C. H. Thoma, "Improved envelope and centroid equations for high current beams," in *Proc. 14th Int. Conf. High-Power Particle Beams*, Jun. 2002, pp. 463–466.
[12] T. P. Hughes, C. B. Mostrum, T. C. Genoni, and C. Thoma, "LAMDA user's manual and reference," Voss Sci. Tech., Albuquerque, NM, USA, Rep. VSL-0707, Apr. 2007.
[13] C. A. Ekdahl, "Modeling ion-focused transport of electron beams with simple beam-envelope simulations," Sandia Nat. Lab., Albuquerque, NM, USA, Rep. SAND-0544, 1986.
[14] S. Humphries, "TRAK charged particle tracking in electric and magnetic fields," in *Computational Accelerator Physics*, R. Ryne, Ed. New York, Ny, USA: American Institute of Physics, 1994, pp. 597–601.
[15] (2013). *Technical Information About the TriComp Series of Codes* [Online]. Available: http://www.fieldp.com
[16] S. Humphries, *Field Solutions on Computers*. Boca Raton, FL, USA: CRC Press, 1997.
[17] C. Thoma, T. P. Hughes, and C. Miller, "Envelope and centroid equations in LAMDA and XTR codes," Voss Sci. Tech., Albuquerque, NM, USA, Rep. VSL-0808, Mar. 2008.
[18] Y. Tang, T. P. Hughes, C. A. Ekdahl, and M. E. Schulze, "Beam clean-up zone calculations for 2.5 MV, 1.4 kA experiments on DARHT-2," in *Proc. 16th IEEE Int. Pulsed Power Conf.*, Albuquerque, NM, USA, Jun. 2007, pp. 1257–1260.
[19] C. Thoma and T. P. Hughes, "A beam-slice algorithm for transport of the DARHT-2 accelerator," in *Proc. Part. Accel. Conf.*, Albuquerque, NM, USA, Jun. 2007, pp. 3411–3413.
[20] H. Bender, C. Carlson, D. Frayer, D. Johnson, K. Jones, A. Meidinger, and C. Ekdahl, "Quasi-anamorphic optical imaging system with tomographic reconstruction for electron beam imaging," *Rev. Sci. Instrum.*, vol. 78, no. 1, pp. 013301-1–013301-8, Jun. 2007.
[21] C. Ekdahl, E. O. Abeyta, P. Aragon, R. Archuleta, R. Bartsch, D. Dalmas, S. Eversole, R. Gallegos, J. Harrison, J. Johnson, E. Jacquez, B. T. McCuistian, N. Montoya, S. Nath, D. Oro, L. Rowton, M. Sanchez, R. Scarpetti, M. Schauer, G. Seitz, M. Bender, W. Broste, C. Carlson, D. Frayer, D. Johnson, A. Tipton, C. Y. Tom, and M. Schulze, "Commissioning the DARHT-II scaled accelerator," in *Proc. IEEE Particle Accel. Conf.*, Albuquerque, NM, USA, Jun. 2007, pp. 2373–2375.
[22] M. Reiser, *Theory and Design of Charged Particle Beams*. New York, NY, UAS: Wiley, 1994, p. 467.
[23] T. P. Wangler, K. R. Crandall, R. Ryne, and T. S. Wang, "Particle-core model for transverse dynamics of beam halo," *Phys. Rev. Special Topics Accel. Beams*, vol. 1, no. 8, pp. 084201-1–084201-9, Dec. 1998.
[24] R. L. Guckstern, "Analytic model for halo formation in high current ion linacs," *Phys. Rev. Lett.*, vol. 73, no. 9, pp. 1247–1250, Aug. 1994.
[25] P. Loschialpo, W. Namkung, M. Reiser, and J. D. Lawson, "Effects of space charge and lens aberrations in the focusing of an electron beam by a solenoid lens," *J. Appl. Phys.*, vol. 57, no. 1, pp. 10–17, Jul. 1985.
[26] S. Bernal, B. Quinn, M. Reiser, and P. G. O'Shea, "Edge imaging in intense beams," *Phys. Rev. Special Topics Accel. Beams*, vol. 5, no. 6, pp. 064202-1–064202-9, Jun. 2002.

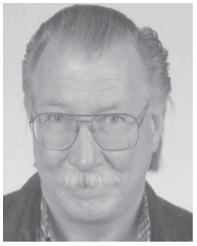

Carl Ekdahl (M'95–SM'13) received the B.A. degree in physics from San Diego State College, San Diego, CA, USA, and the M.S. and Ph.D. degrees in physics from the University of California at San Diego, La Jolla, CA.

He has practiced experimental physics with Smyth Research Associates and the Scripps Institution of Oceanography, San Diego, CA, Mission Research Corporation, and Sandia National Laboratories, Albuquerque, NM, USA, and the Los Alamos National Laboratory, Los Alamos, NM. He is currently pursuing further improvements to beam quality on the DARHT-II long-pulse linear induction accelerator with the Los Alamos National Laboratory. His current research interests include accelerators and intense relativistic electron beams, high energy density plasmas, warm dense matter, and high energy density hydrodynamics.

Dr. Ekdahl is a member of the American Physical Society Division of Beams and Plasma Physics. He serves on the International Advisory Committee for the High Power Particle Beam Conferences. He served on various IEEE award and conference organizing committees and he is currently the Senior Editor for the Charged Particle Beams and Sources Technical Area of the IEEE TRANSACTIONS ON PLASMA SCIENCE.